AIAA JOURNAL
Vol. 30, No. 2, February 1992

Heat Removal in a Gas Cooled Solid-State Laser Disk Amplifier

S. B. Sutton,* G. F. Albrecht,* and H. F. Robey*
Lawrence Livermore National Laboratory, Livermore, California 94550

The flow, heat transfer, and optical characteristics of the gas cooled slab solid-state disk laser geometry are experimentally and numerically addressed. Such a configuration has applications in solid-state laser fusion drivers. Data on viscous and thermal boundary-layer development in an asymmetrically heated channel are presented showing the large cooling variations that occur during thermal development. The flow related cooling variations are then directly related to optical distortions in the laser slab. It is shown that the flow can be properly conditioned such that the optical distortions due to cooling effects will be small enough to make average power solid-state laser fusion drivers possible.

I. Introduction

IN recent years, there has been a resurgence of interest in high average power solid-state lasers,[1,2] including their application as a driver for an inertial confinement fusion (ICF) reactor. Since, for flash-lamp pumped systems, at least one unit of heat is deposited in the laser material for every unit of optical energy extracted, it has been presumed that the usefulness of a solid-state laser driver would be severely limited by the effect that variations in heat removal have on laser beam quality. Past studies[2,3] discussed this issue and identified the gas cooled slab (GCS) disk amplifier as having the potential to achieve megawatt power levels at acceptable laser beam qualities. A recent study addressed efficiency optimization of GCS laser systems.[4]

The basic GCS geometry is shown in Fig. 1. The amplifier consists of several laser slabs oriented at Brewster's angle, following the standard convention for large aperture solid-state laser amplifiers.[5] The slabs are energy pumped from the top and bottom using flash lamps or, in the future, diode laser panels. Each laser slab is sandwiched between two flow separation windows. To remove the waste heat deposited in the slab by the pumping and lasing processes, a cooling gas flows over the faces of the slab confined in a channel formed by the slab face and a flow separation window. The flow separation window separates the high-velocity cooling flow from a much slower flow that may be present in the drift regions. The flow direction is toward the plane of Fig. 1, with a cross section given in Fig. 2. Upstream of the slab, there may be a viscous and thermal development region where the flow is conditioned prior to contacting the laser slab.

Since variations in the slab temperature across the aperture result in optical distortions in the laser beam, understanding the flow and heat removal characteristics is critical to specifying a flow geometry that in the end achieves acceptable wave-front quality of the output beam. Particularly important is the impact that highly nonlinear temperature variations have on optical distortions. Such non-linear variations occur in developing boundary layers.

Several previous studies have addressed some aspects of entrance effects in turbulent planar channel flow.[6-9] The recent numerical simulations of Crawford and Pietrzyk[9] showed the effects of entrance conditions and Reynolds number on heat transfer characteristics at the channel entrance. In this paper, we extend this work to further quantify the entrance region heat transfer characteristics and relate them to optical distortions in the laser slab.

II. Flow and Heat Transfer in the Cooling Channel

Referring again to Fig. 2, each of the two cooling streams exits a plenum through a fine mesh screen assembly, flows through an asymmetric nozzle, then encounters the channel. The screen is used to both eliminate large-scale turbulent structures and create uniform flow at the plenum exit. Starting at the nozzle exit, viscous boundary layers form on both channel walls, thicken with downstream distance, and eventually merge, producing a fully developed velocity profile. In the channel region, there are asymmetric thermal boundary conditions. On the flow separation window side, the thermal boundary condition is nearly adiabatic. On the laser slab side of the channel, a thermal boundary layer starts forming at the first location where heat is applied to the flow. This can be either at the leading edge of the slab or someplace in the upstream conditioning region if external heating is applied. The thermal boundary layer grows with downstream distance, eventually filling the entire channel. The temperature profile will then remain largely unchanged and can be considered fully developed. Variations in the slab temperature associated with growth of the thermal boundary layer will be shown in Sec. III to have an important effect on optical distortions.

Both the viscous and thermal transport characteristics of the cooling channel flow must be modeled so that the proper boundary conditions can be applied in calculating optical distortions. The TEXSTAN[10] boundary-layer computer program was used to numerically calculate the viscous and thermal development. The program incorporates a two-equation turbulence model[9,11] with near wall damping effects, which are

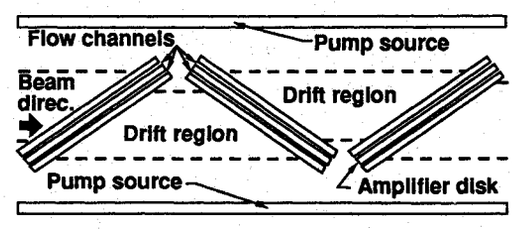

Fig. 1 Schematic of a gas cooled slab amplifier showing the inclined slabs, flow separation windows, and cooling flow channels.

Received April 26, 1990; revision received Dec. 28, 1990; accepted for publication Feb. 15, 1991.

*Advanced Applications Program, P.O. Box 808.

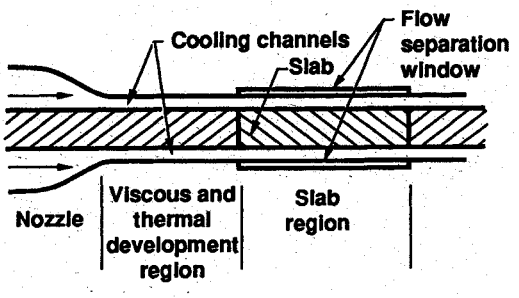

Fig. 2 Slice through an amplifier disk assembly of Fig. 1 showing the cooling flow geometry.

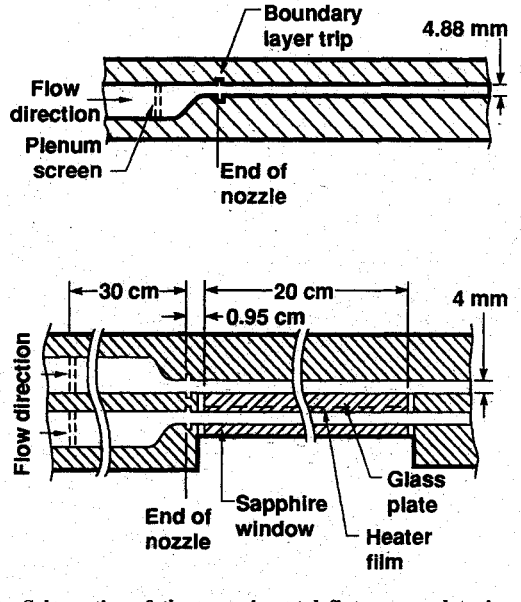

Fig. 3 Schematics of the experimental fixtures used to investigate viscous boundary-layer development and thermal boundary layer development: a) viscous development fixture; b) thermal development fixture.

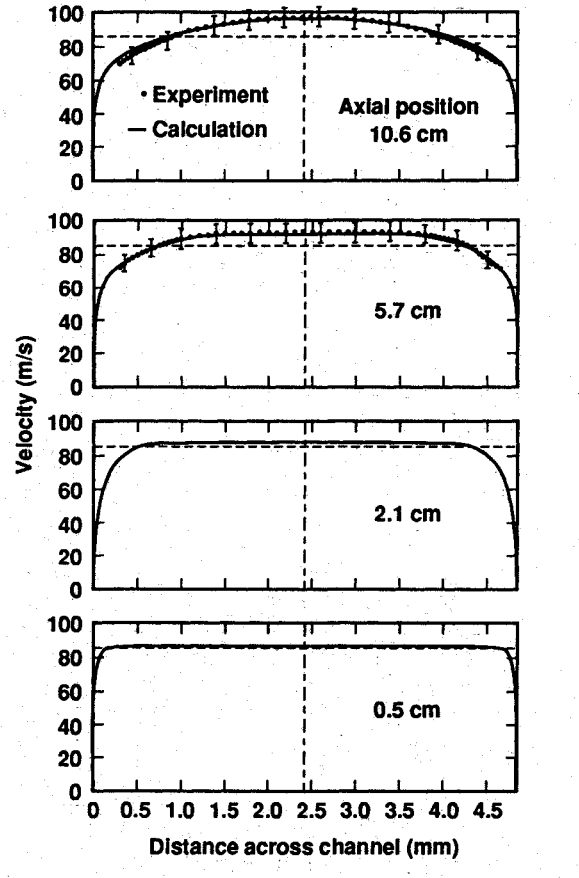

Fig. 4 Calculated and measured velocity profiles in the viscous development fixture at a nozzle exit velocity of 84.8 m/s.

particularly important during the early growth portion of the viscous boundary layer.

Several experiments were performed to provide insight into the flow and heat transfer characteristics and provide data for validation of the numerical model. The experimental fixtures, schematically shown in Figs. 3, replicated the geometry shown in Fig. 2. Channel thicknesses and nozzle shapes are representative of those that would be used in an actual device.[4] The first fixture, which had only a single channel (Fig. 3a), was employed to characterize viscous development. At several axial locations, there are penetration ports for inserting a hot-wire probe to measure the velocity profile. Because the presence of penetration ports interferes with either a heating film or optical diagnostics, a second fixture (Fig. 3b) was required to study thermal boundary-layer development. Dry nitrogen was used for the cooling fluid in both experiments.

In the viscous development fixture (Fig. 3a), there was a negligibly small distance between the fine mesh screen and the nozzle entrance. Thus, the flow entered the nozzle with thin boundary layers. The boundary layers were further thinned in the nozzle because of the strong streamwise favorable pressure gradient, resulting in a uniform flow condition at the nozzle exit. The velocity profile across the channel was measured at several streamwise locations using a constant temperature hot-wire anemometer. A boundary-layer probe, with a 4-μm-diam element, was mounted to a micrometer traverse, which allowed the probe to be accurately positioned across the channel to within 0.2 mm of the walls. Uncertainty in the position and calibration errors results in a total measurement error of 6.5%. Calculated velocity profiles at four axial locations (measured from the end of the nozzle) and the corresponding measured velocity profiles at two locations are shown in Fig. 4. In this figure, the vertical dashed line denotes the channel center and the horizontal dashed lines denote the equivalent uniform velocity. The nozzle exit velocity and pressure were determined to be 84.8 m/s and 2 atm, respectively. The resulting Mach number and Reynolds number (based on this flow velocity and the hydraulic diameter, which is twice the channel thickness) were 0.24 and 1.055×10^5, respectively. Both of these values are at the upper limit of flow conditions envisioned for an operating device.[4] The flow is seen to be symmetric and accelerates in the center, demanded by continuity, as the flow evolves. There is excellent agreement between the calculations and experimental data.

In the thermal development fixture (Fig. 3b), the nozzle entrance was 0.26 m downstream of the plenum screen. The added development length upstream of the nozzle resulted in thick boundary layers entering the nozzle. The boundary layers, after thinning in the nozzle, were calculated to occupy 35% of the channel thickness at the nozzle exit. This is considerably thicker than in the fixture used to measure viscous development. In this experiment, only the centerline velocity, static pressure, and centerline turbulent intensity were measured at the nozzle exit; the values were 47 m/s, 2.06 atm, and 0.45%, respectively. The Reynolds number and Mach number for the flow were 4.93×10^4 and 0.13, respectively. These values are representative of those envisioned for an operating device.[4] The modified Froude number[12] based on the channel thickness and the maximum anticipated temperature drop across the channel thermal boundary layer is over 2×10^5. This is sufficiently large to make buoyancy effects negligible compared to inertial or viscous effects.

As noted in Fig. 3b, heating was accomplished through a 0.1-mm-thick inconel film heater attached to one surface of the glass plate placed in the center dividing vane. The heater

started 1 cm downstream of the nozzle exit. The glass plate was supported in the surrounding aluminum plate by a 0.3-cm-thick layer of elastomer (measured thermal conductivity of 0.69 W/m-K). Since the center divider was cooled on both sides, the portion of the applied heat flux, which conducted through the glass substrate (thermal conductivity of 1.0 W/m-K), was removed by the flow in the opposite channel. It is calculated that, for the conditions considered, 72–76% of the heat was removed by flow in the channel directly exposed to the heater film.

The surface temperature distribution was measured using a Hughes Probeye infrared camera for two values of heat flux: 1.0 and 1.5 W/cm^2 (corrected to 0.75 and 1.13 W/cm^2 removed by the flow directly exposed to the heater film). The heated surface, which was painted black to maximize the emissivity, was viewed through a 4-mm-thick sapphire window mounted in the outer wall of the flow channel. The uncertainty in the Probeye temperature measurements is estimated to be ±1.0°C for surface temperatures above 40°C. For temperatures below 40°C, the error increases (±3.0°C at room temperature) as the background IR environment becomes more significant.

Additional measurement errors are associated with measurement of flow properties and resolution of the Probeye. The latter introduces a flow direction positional uncertainty associated with resolution in the camera image and uncertainty in the actual position of the image. This uncertainty is estimated to range from ±2 mm in the high-gradient boundary-layer growth region to ±5 mm in the downstream portions where the surface temperature gradient is nearly linear. The pressure, temperature, and velocity of the gas in the flow channel and the heat flux applied to the heater were measured with accuracies estimated to be ±1.5%, ±0.2°C, ±2%, and ±1%, respectively. An rms summation of these individual errors results in an error in the measured temperature estimated to be ±2.4°C over most of the plate. The error is slightly larger in the high-gradient portion of the profile.

The measured and calculated surface temperatures are given in Fig. 5. Experimental error bars are given on several points. The surface temperature undergoes an abrupt rise starting at the leading edge of the slab, then makes a gradual transition to a nearly constant gradient at the downstream extent of the slab. For the conditions considered, this transition is at least 5 cm in length, or about 12 channel thicknesses. Variations in the initial region are associated with development of the thermal boundary layer. Once the thermal boundary layer has become fully developed, a linear increase in the surface temperature results from an increase in the bulk (or average) fluid temperature in response to the added heat. Additionally, there is the noticeable drop in the experimentally measured temperature at the trailing edge of the slab. This is the result of conduction, through the elastomer bond, to the colder unheated support frame.

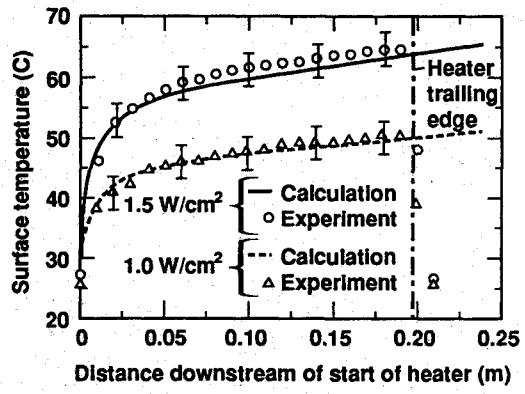

Fig. 5 Surface temperature variation in a developing boundary layer: experimental values and numerical predictions for surface heat flux values of 1.0 and 1.5 W/cm^2.

The calculated surface temperature variation is seen to compare well with the measured values. This excellent agreement between the calculations and the measured data indicate that the numerical model is capable of quantitative predictions of heat transfer in an asymmetrically heated channel. These calculations also show the strong variation in cooling parameters present during thermal boundary-layer development.

If an optical aperture of 10 cm were located between 0 and 0.1 m in Fig. 5, the thermal development region would encompass 50% of the aperture. Since optical distortions track the surface temperature variations, as will be shown in the next section, it is important to minimize temperature variations in the slab, particularly those that are highly nonlinear. This can be accomplished by either shortening the development length if development starts at the leading edge of the slab or thermally conditioning the flow upstream of the slab so that development takes place outside of the aperture. Shortening the development length is still an important issue if thermal conditioning is used. Reducing the thermal development length would reduce the efficiency penalty associated with auxiliary surface heaters in an integrated laser amplifier system.

Previous calculations[9] have been reported that suggested that having thin boundary layers at the nozzle exit and having viscous and thermal development start simultaneously (no offset) could substantially shorten the thermal development length. Additional calculations have been performed that substantiate this observation. Figure 6 demonstrates the sensitivity of the thermal development length to viscous conditioning prior to heating. This figure compares surface temperature and convection heat transfer coefficient for two cases: simultaneous development of the viscous and thermal boundary layers, and 1 cm (2.5 channel thicknesses) of viscous development upstream of the leading edge of the heater. In the latter case, the viscous boundary layers occupied 15% of the channel at the start of heating. The length of the highly nonlinear development region is reduced by as much as 40% if the viscous and thermal boundary layers develop simultaneously.

III. Optical Distortions in the Laser Slab

Variations in the slab temperature will result in degradation of laser beam quality as measured by the variation in the optical path length over the aperture. The total optical path length of a light ray after it travels through the slab is the integral of the index of refraction along the path of the ray. Variations in index of refraction arise from variations in temperature T and stress as follows:

$$n = n_0 + \frac{\partial n}{\partial T}\Delta T + \frac{\partial n}{\partial \sigma}\Delta\sigma \qquad (1)$$

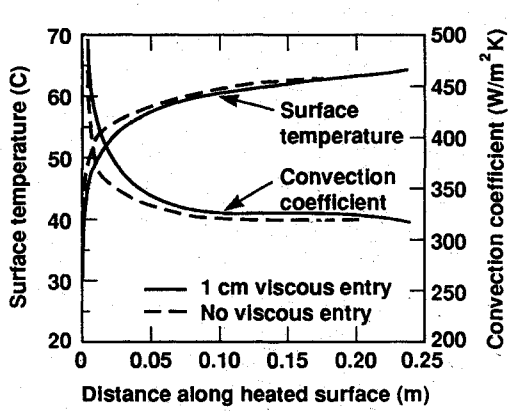

Fig. 6 Effect of viscous preconditioning on surface temperature gradients and the convective heat transfer coefficient.

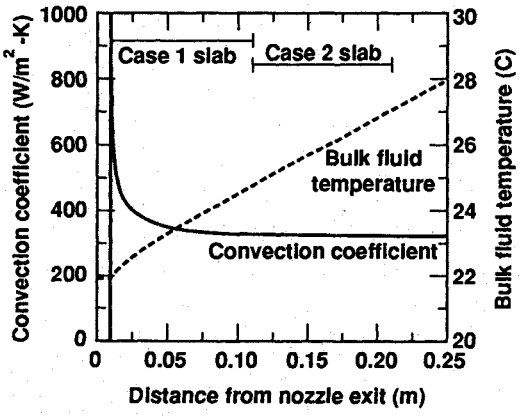

Fig. 7 Convection coefficient and bulk fluid temperature variation for the 1-cm viscous entry case of Fig. 6.

where n is the index of refraction, n_0 the index at a given reference temperature and zero stress, σ the stress tensor, $\partial n/\partial\sigma$ the stress-optic tensor, and $\partial n/\partial T$ the temperature coefficient. The elements of the stress optic tensor and the temperature coefficient are material constants. Three effects are thus seen to enter into optical path length variations: temperature effects on the index of refraction, stress effects on the index of refraction, and bulk thermal expansion affecting the total path length. Since the flow is uniform in the direction transverse to the flow, temperature variations occur only in the flow direction. The LASRPAK[13–15] codes were used to calculate the thermomechanical stress and optical distortions in the laser slab subject to convective cooling on the slab faces. There are three calculations in the sequence. First, the thermal transport portion of the package solves the steady-state heat conduction equation, including energy deposition associated with the energy pumping and lasing processes. This is followed by the solution of the mechanics equations for the resulting stress and displacement fields. Once the temperature, stress, and displacement fields have been determined, optical path variations are calculated.

Calculations were performed for a slab made of a phosphate glass (thermal conductivity: 0.85 W/m-K, thermal expansion coefficient: 7.7×10^{-6}/C, elastic modulus: 7×10^{10} Pa, Poisson's ratio: 0.23, refractive index: 1.53). The slab is $10 \times 18 \times 0.7$ cm thick, with cooling flow in the 10-cm direction. Thermal conditions were taken from the 1-cm viscous entry case of Fig. 6. The convective heat transfer coefficient and bulk fluid temperature are given in Fig. 7. The surface temperature tracks closely to that given in Fig. 6. The sudden increase in convection coefficient at 1 cm downstream of the nozzle indicates the start of heating. In the subsequent figures, two slab locations are considered, indicated in Fig. 7 as case 1 and case 2. In case 1, the slab starts at 1 cm downstream of the nozzle exit and extends for a distance of 10 cm. In case 2, 10 cm of auxiliary surface heater is used to thermally condition the flow upstream of the slab. In this instance, the heater starts at 1 cm downstream of the nozzle exit and the slab starts at 11 cm downstream of the nozzle exit. In both calculations, the perimeter edges of the slab were adiabatic.

Changes in the phase of the beam are typically used to quantify changes in the optical path length. Within the optics community, phase variations are also referred to as wave-front distortion. The resulting changes in the phase of the beam along a slice taken in the flow direction are given in Figs. 8. The total phase displacement, as well as the individual contributions due to temperature and stress effects on the index of refraction and bulk growth in the material, are given. Consider first Fig. 8a, which is for the case 1 slab of Fig. 7. There are three distinct regions along the width, i.e., along the cooling flow direction. Between about 0.04 and 0.08 m the wave-front variation is reasonably linear with distance.

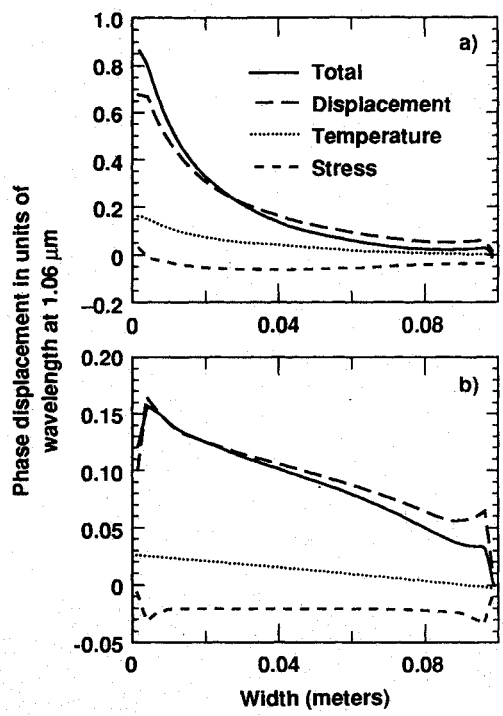

Fig. 8 Wave-front distortion in the laser beam: a) no upstream thermal conditioning; b) 10-cm thermal conditioning length.

Referring to Fig. 7, this is a region where the convection coefficient is nearly constant and the rise in the cooling fluid temperature is linear. Remember that these conditions apply after the thermal boundary layer has become fully developed. The change in wave front in this region is primarily associated with the linear increase in bulk temperature of the cooling fluid. Left of this region (0.01–0.04 m), there is a large nonlinear variation in the wave front, associated with the strong variation in the convective heat transfer coefficient. Considering the individual effects that contribute to the wave-front distortion, it is clear that bulk distortion (thermal expansion) dominates. The next most important component is the temperature effect on the index of refraction. Stress effects over the central portion of the slab (0.01–0.09 m) are insignificant. Finally, since the wave-front distortion appears to mimic the cooling variations, thermal conduction within the slab does little to mitigate the cooling effects.

Now consider Fig. 8b, which is for the case 2 slab of Fig. 7, and focus on the central 80% of the slab extending from 0.01 to 0.09 m. To either side of this region are zones where end effects dominate the wave-front distortion. In this central region, the wave-front variation is nearly linear. This is to be expected since the convection coefficient is almost constant and the bulk temperature of the cooling fluid varies linearly. Over the central portion of the slab (0.01–0.08 m), the total wave-front variation is over a factor of 4 less than in the first case (Fig. 8a).

These results indicate that optical distortion in the slab is primarily due to thermal expansion through the thickness and that the shape tracks variations in the heat transfer coefficient. In order to minimize the optical distortion, it is a simple matter to place development of the thermal boundary layer upstream of the laser slab using resistive heaters.

The wavefront distortion is a combination of linear and nonlinear contributions. In practice, the simple beam tilt from the linear contribution is trivially alleviated by an appropriate displacement of optical components, leaving only the nonlinear effect. From Fig. 8a, if no thermal conditioning is employed, the nonlinear contribution is of order 0.2 waves. If, on the other hand, thermal conditioning is used, the nonlinear distortions (Fig. 8b) are of order 0.01 waves. In actual operating lasers, the thermal load could be as much as a factor

of 5 greater than considered in these calculations, resulting in of order 1 wave without thermal conditioning and 0.05 waves with thermal conditioning.

Efficient laser extraction would require 10–20 slabs per amplifier module. The resulting nonlinear contributions in case 2 (Fig. 8b) would add up to of order 0.5 waves, which is of no practical concern and can be removed with adaptive optics. In case 1 (Fig. 8a), the nonlinear contribution adds to of order 10 waves per module, which is sufficient to redirect the rays within one amplifier module. This makes beam transport difficult, if not impossible.

IV. Summary and Conclusions

The cooling of average power solid-state laser disks has been discussed, focusing on the influence of the cooling flow on optical distortion in the laser slab. Experiments and calculations, detailing development of the viscous and thermal boundary layers in an asymmetrically heated plane channel, have been described. The excellent agreement between calculations and experimental results demonstrates that the numerical model used can accurately simulate developing channel flows. The heat transfer calculations provided boundary conditions for calculations that detailed the thermally induced optical distortions in a representative laser amplifier disk. Several important conclusions result from this study. Stress-optic calculations show that optical distortions track heat transfer variations associated with thermal boundary-layer development. Without thermal conditioning upstream of the laser slab, the thermal development region can encompass a significant portion of the laser aperture. In this case, the uncorrected nonlinear optical distortion for an amplifier module is of order 10 waves. With proper upstream thermal conditioning, the uncorrected nonlinear optical distortion can be reduced by as much as a factor of 20 below the value associated with no upstream thermal conditioning. This makes thermal conditioning outside of the optical aperture a necessity. These results, in conjunction with other findings,[4] verify that the gas cooled slab geometry is a viable approach for large aperture average power solid-state lasers.

Acknowledgments

This work was performed under the auspices of the U.S. Department of Energy by the Lawrence Livermore National Laboratory under Contract W-7405-Eng-48. The authors gratefully acknowledge the expert assistance of Barry Freitas, the willingness of Said Doss and Robert Gelinas to modify their stress-optics codes for the GCS geometry, and Michael Crawford of the University of Texas for the use of the TEXSTAN computer program.

References

[1]Emmett, J. L., Krupke, W. F., and Trenholme, J. B., *Physics of Laser Fusion*, Volume IV, The Future Development of High-Power Solid State Laser Systems, Lawrence Livermore National Lab., UCRL-53344, Livermore, CA, Nov. 1982.

[2]Emmett, J. L., Krupke, W. F., and Sooy, W. R., "The Potential of Average-Power Solid State Lasers," Lawrence Livermore National Lab., UCRL-53571, Livermore, CA, Sept. 1984.

[3]Albrecht, G. F., and Sutton, S. B., "Gas Cooling of Laser Disks," Energy and Technology Review, Lawrence Livermore National Lab., UCRL-52000-88-5, Livermore, CA, May 1988, pp. 25–34.

[4]Sutton, S. B., and Albrecht, G. F., "Optimum Performance Considerations for a Large Aperture Average Power Solid State Laser Amplifier," *Journal of Applied Physics*, Vol. 69, No. 3, 1991, pp. 1183–1191.

[5]Murray, J. E., Powell, H. T., and Woods, B. W., "Optimized Flashlamp Pumping of Disc Amplifiers," *Proceedings of the Society of Photo-Optical Instrumentation Engineers*, Vol. 609, 1986, pp. 95–110.

[6]Boelter, L. M., Young, G., and Iverson, H. W., "An Investigation of Aircraft Heaters. XXVII—Distribution of Heat Transfer Rate in the Entrance Section of a Circular Tube," National Advisory Committee for Aeronautics, TN-1451, University of California, Berkeley, CA, July 1948.

[7]Quarmby, A., "Some Measurements of Turbulent Heat Transfer in the Thermal Entrance Region of Concentric Annuli," *International Journal of Heat and Mass Transfer*, Vol. 10, No. 3, 1967, pp. 267–276.

[8]Bradshaw, P., Dean, R. B., and McEligot, D. M., "Calculation of Interacting Turbulent Shear Layers: Duct Flow," *Journal of Fluids Engineering*, Vol. 95, No. 2, 1973, pp. 214–220.

[9]Crawford, M. E., and Pietrzyk, J. R., "Numerical Simulation of Turbulent Convective Heat Transfer in the Entry Region of an Asymmetrically-Heated Planar Channel with Application to Gas-Cooled Laser Slabs," Kaiser Engineers Corp., Oakland, CA, Dec. 1986.

[10]Crawford, M. E., and Kays, W. M., "STAN5—A Program for Numerical Computation of Two-Dimensional Internal and External Boundary Layer Flow," NASA CR-2742, Nov. 1976.

[11]Chien, K.-Y., "Predictions of Channel and Boundary-Layer Flows with a Low-Reynolds-Number Turbulence Model," *AIAA Journal*, Vol. 20, No.1, 1982, pp. 33–38.

[12]Meroney, R. N., Neff, D. E., and Cermak, J. E., "Wind Tunnel Modeling of LNG Spills," *Proceedings of the American Gas Association Transmission Conf.*, 1978, pp. T217–T223.

[13]Gelinas, R. J., Doss, S. K., Murty, S. S., and Trenholme, J. B., "Heat Transfer in Solid State Laser Systems: Applications of Dynamic ADI Methods," *International Journal of Numerical Methods in Engineering*, Vol. 24, Jan. 1987, pp. 177–202.

[14]Doss, S. K., "Physics and Mathematics of the BREW Code," *1986 Laser Program Annual Report*, Lawrence Livermore National Lab., UCRL-50021-86, Livermore, CA, Nov. 1987, pp. 7-132–7-135.

[15]Gelinas, R. J., "Model Analysis of Optical Path Differences in Pumped Zig-Zag Slabs," *1986 Laser Program Annual Report*, Lawrence Livermore National Lab., UCRL-50021-86, Livermore, CA, Nov. 1987, pp. 7-139–7-142.